ACS Chemical Biology

Articles

pubs.acs.org/acschemicalbiology

N-Myristoyltransferase Inhibition Induces ER-Stress, Cell Cycle Arrest, and Apoptosis in Cancer Cells

Emmanuelle Thinon,[†,‡,∥] Julia Morales-Sanfrutos,[†] David J. Mann,[‡,§] and Edward W. Tate*[,†,§]

[†]Department of Chemistry, Imperial College London, Exhibition Road, London SW72AZ, United Kingdom

[‡]Department of Life Sciences, Imperial College London, Exhibition Road, London SW72AZ, United Kingdom

[§]Institute of Chemical Biology, Department of Chemistry, Imperial College London, Exhibition Road, London SW72AZ, United Kingdom

Supporting Information

ABSTRACT: *N*-Myristoyltransferase (NMT) covalently attaches a C14 fatty acid to the N-terminal glycine of proteins and has been proposed as a therapeutic target in cancer. We have recently shown that selective NMT inhibition leads to dose-responsive loss of *N*-myristoylation on more than 100 protein targets in cells, and cytotoxicity in cancer cells. *N*-myristoylation lies upstream of multiple pro-proliferative and oncogenic pathways, but to date the complex substrate specificity of NMT has limited determination of which diseases are most likely to respond to a selective NMT inhibitor. We describe here the phenotype of NMT inhibition in HeLa cells and show that cells die through apoptosis following or concurrent with accumulation in the G1 phase. We used quantitative proteomics to map protein expression changes for more than 2700 proteins in response to treatment with an NMT inhibitor in HeLa cells and observed down-regulation of proteins involved in cell cycle regulation and up-regulation of proteins involved in the endoplasmic reticulum stress and unfolded protein response, with similar results in breast (MCF-7, MDA-MB-231) and colon (HCT116) cancer cell lines. This study describes the cellular response to NMT inhibition at the proteome level and provides a starting point for selective targeting of specific diseases with NMT inhibitors, potentially in combination with other targeted agents.

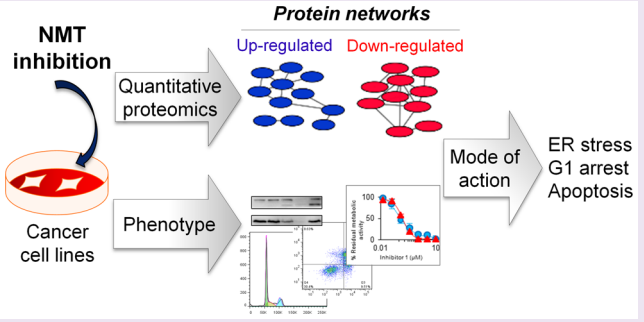

N-myristoylation is the irreversible attachment of a C14 fatty acid to the N-terminal glycine of a protein, catalyzed by myristoyl CoA: protein *N*-myristoyltransferase (NMT).[1,2] Although the majority of *N*-myristoylation occurs cotranslationally, we recently identified at least 30 proteins that are myristoylated post-translationally during apoptosis, where cleavage of proteins by caspases reveals a new N-terminal glycine.[3] *N*-myristoylation has been shown to be important for the viability and survival of many organisms, including plants, parasites, and humans, and NMT is an actively investigated therapeutic target in parasite and fungal infections.[4−14] In humans, the two homologues of NMT, HsNMT1 and HsNMT2,[15] are potential chemotherapeutic targets in cancer and autoimmune disorders[16] and have been shown to be up-regulated in several cancers.[2,17,18] Chemical proteomic approaches[19] have recently revolutionized the ability to profile the substrates of lipid transferases such as NMT in cells and in intact vertebrates,[20] enabling new approaches for drug target discovery and validation based on complete and quantitative knowledge of the response of the lipidated proteome to transferase inhibitors *in vivo*.

We recently characterized a selective HsNMT inhibitor (compound **1**, Figure 1A), a molecule originally discovered as an inhibitor of *Trypanosoma brucei* NMT, as a tool to study NMT inhibition in mammalian cells.[3] We demonstrated that this compound acts on-target in HeLa cells, causing dose-dependent inhibition of *N*-myristoylation that is cytotoxic in a time-dependent manner. Interestingly, HeLa cells maintain a "plateau" of residual metabolic activity (approximately 25% of untreated levels) following 3 days of inhibition even in the presence of concentrations of inhibitor **1** (from 1 μM to 10 μM) that deliver complete inhibition of *N*-myristoylation in cells (Supporting Information Figure 1). This plateau drops with extended exposure, resulting in complete killing of HeLa cells following 7 days of exposure. Using a chemical proteomic method, we generated comprehensive and quantitative profiles of NMT substrates, and their response to NMT inhibition; a total of 70 cotranslational and 30 post-translational NMT substrates were identified in HeLa cells,[3] and similar analyses were subsequently applied to other cell lines and an intact vertebrate organism.[20] These substrates encompass a rich variety of functions in cells; *N*-myristoylation is known to be important for localization and function in some cases, such as the proto-oncogene c-Src,[21] AMP-dependent kinase,[22] or 26S

Received: April 28, 2016
Accepted: May 24, 2016
Published: June 7, 2016

DOI: 10.1021/acschembio.6b00371
ACS Chem. Biol. 2016, 11, 2165−2176

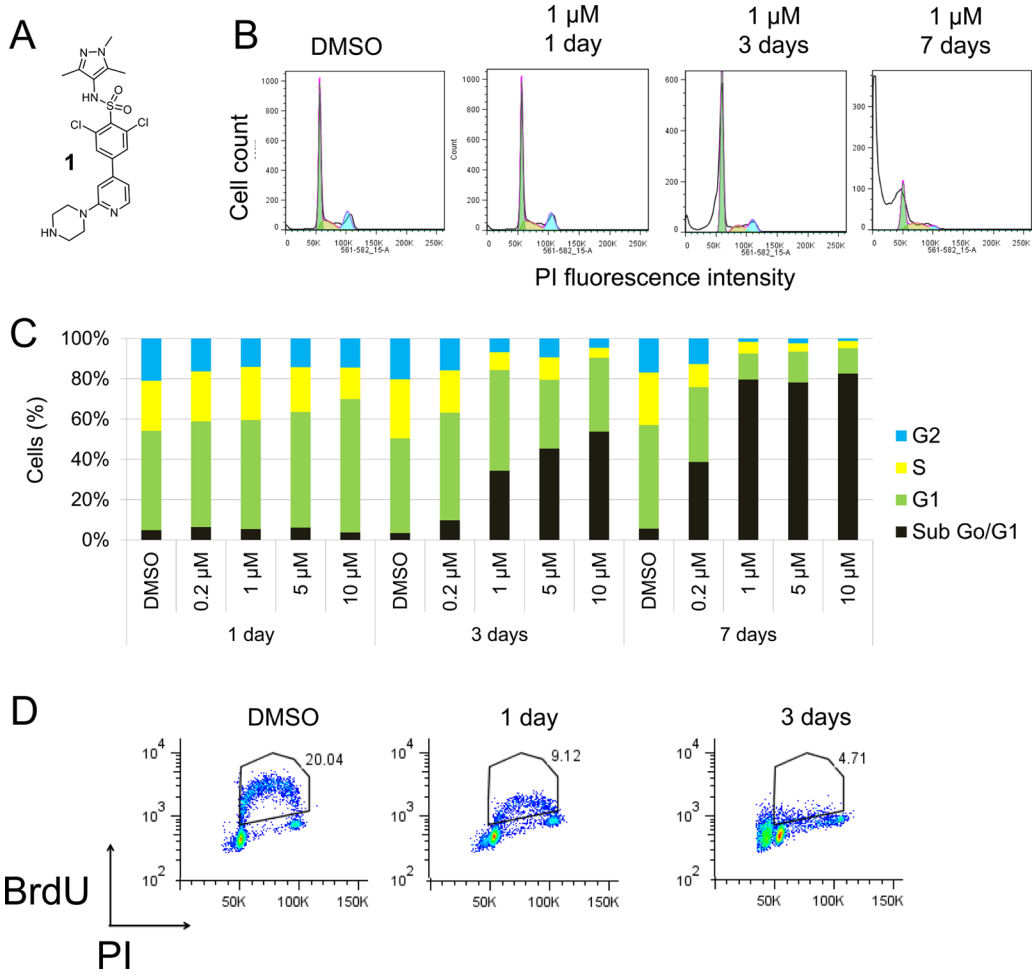

Figure 1. NMT inhibition induced G1 arrest in HeLa cells. (A) Structure of compound **1**. (B) Representative DNA content analysis for treatment with DMSO (vehicle) or 1 μM inhibitor **1** for 1, 3, or 7 days. DNA was stained with propidium iodide (PI) and DNA content determined by flow cytometry. Number of cells was plotted against the PI fluorescence intensity. (C) Cell cycle analysis (n = 3 biological replicates, SEM < 10%) across a range of inhibitor concentrations and time points. The data were analyzed with FlowJo. (D) Flow cytometry experiment of cells treated with bromodeoxyuridine (BrdU) and PI following treatment with DMSO or inhibitor **1** (5 μM) for 1 or 3 days.

proteasome regulatory subunits.[23,24] Several substrates have also been linked to cancer progression such as nucleolar protein 3, whose overexpression has been associated with cancer cell resistance to apoptosis.[25] These results suggest that inhibition of *N*-myristoylation affects multiple biological pathways, ultimately resulting in cell death in cancer cell lines.

In recent years, quantitative proteomics has become a powerful tool to study the mode of action of drugs[26,27] since it provides a relatively unbiased assessment of functional changes occurring at the protein level and takes into account important functional alterations such as changes in post-translational events or protein degradation rate that are not directly accessible to nucleic acid sequencing technology.[26] A quantitative proteomics approach could be particularly informative for determining the mode of action for inhibition of an enzyme with multiple substrates and that thus induces multiple simultaneous downstream effects. In this study, we applied quantitative proteomics to study proteome level effects of NMT inhibition on HeLa cells, characterize the cytotoxic phenotype, and identify top-level pathways that are modulated by NMT inhibition. These data provide a starting point for future studies to decipher the mode of action of NMT inhibitors in specific disease contexts and for validation of human NMT as a therapeutic target through identification of sensitive disease subtypes or novel drug combinations.

RESULTS

NMT Inhibition Impacts Cell Cycle through G1 Arrest.

We sought to investigate the response of cancer cells to compound **1** in more detail to aid understanding of the mechanism of action of this selective NMT inhibitor. The effect of NMT inhibition on cell proliferation and apoptosis was evaluated in HeLa cells treated with various concentrations of inhibitor **1** or with vehicle (DMSO) for 1, 3, or 7 days. 0.2 μM inhibitor **1** corresponds to the EC_{50} value measured by a standard metabolic activity (MTS) assay.[3] As demonstrated by previous tagging analyses, 0.2 μM and 1 μM inhibitor correspond to concentrations sufficient to inhibit 50% and 90% NMT activity in HeLa cells, while treatment with 5 μM or 10 μM results in undetectable NMT activity in cells.[3] Complete NMT inhibition results in the previously observed plateau of residual metabolic activity in an MTS assay after 3 days (Supporting Information Figure 1). After 1 day, samples treated with 1, 5, or 10 μM inhibitor displayed a significant G1 accumulation (p < 0.01; Figure 1B and C). After 3 days, a substantial proportion of cells treated with 1 μM or greater

DOI: 10.1021/acschembio.6b00371
ACS Chem. Biol. 2016, 11, 2165−2176

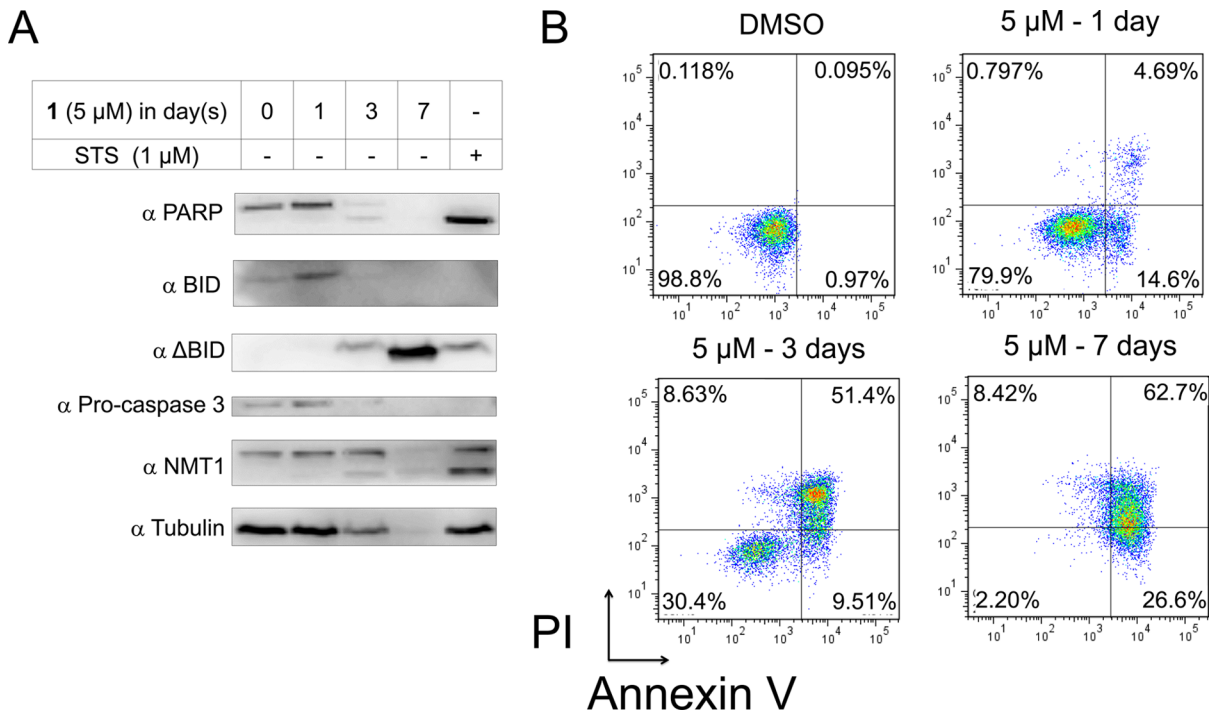

Figure 2. Prolonged NMT inhibition induces apoptosis in HeLa cells. (A) Western blot analysis of apoptotic markers in HeLa cells treated for 0, 1, 3, or 7 days with 5 μM inhibitor **1**. Cells were treated with staurosporine (STS) (1 μM) for 4 h as a control for apoptosis. (B) Flow cytometry analyses of cells treated with Annexin V and PI following treatment with inhibitor **1**.

inhibitor concentration were sub-G1 (dead/apoptotic), with the remainder mainly arrested in the G1 phase. Following 7 days of inhibition, cells were mostly dead/apoptotic (sub-G1) in samples treated with >1 μM of inhibitor, whereas ca. 40% of cells treated with 0.2 μM inhibitor were dead after 7 days, consistent with the MTS assay (Supporting Information Figure 1). These findings suggest that upon NMT inhibition cells undergo G1 arrest followed by cell death. Selective NMT inhibition is characterized by a progressive onset of cytotoxicity, and we hypothesized that this is due to the time required to turn over existing *N*-myristoylated proteins in cells, concurrent with evolution of the proteome toward a predominance of nonmyristoylated NMT substrates. To confirm the observed cell cycle arrest phenotype, cells were stained with BrdU/PI and analyzed by flow cytometry (Figure 1D and Supporting Information Figure 2). BrdU staining after 1- and 3-day treatments with inhibitor **1** indicated a substantial decrease in DNA synthesis, confirming that cells arrested.

NMT Inhibition Induces Apoptotic Cell Death in a Specific Time Frame. To investigate the mode of cell death, markers of apoptosis were analyzed by Western blot in HeLa cells treated for 1, 3, or 7 days with inhibitor **1** (Figure 2A). Staurosporine (STS), a nonspecific kinase inhibitor known to induce apoptosis,[28] was used as a positive control for apoptosis, and HsNMT1, which was previously shown to be cleaved during apoptosis,[29] was also assessed. Markers of apoptosis did not change after 1 day of inhibition in agreement with cell cytotoxicity[3] and cell cycle analyses (Figure 1C). However, at 3 days treatment, PARP, BID, Caspase 3, and HsNMT1 were all cleaved to a substantial extent. After 7 days of inhibition, it proved difficult to detect full length or cleaved PARP, HsNMT1, and Caspase 3, probably because of complete degradation. These results suggested that HeLa cells were dying at least in part through apoptosis.

An annexin V-FITC/PI dual staining assay was used to confirm whether inhibitor **1** could induce apoptosis in HeLa cells (Figure 2B and Supporting Information Figure 3). Treatment with inhibitor **1** showed that annexin-V-positive cells increased in a time-dependent manner in response to NMT inhibition. Early apoptotic cells appeared after 24 h treatment, consistent with relocation of phosphatidylserine being a relatively early event in the apoptotic cascade. There was a substantial population of dead cells observed after 3 days of treatment, and all cells stained positive for annexin V after 7 days of treatment, consistent with cell cycle analysis (Figure 1C) and MTS assay. Thus, taken together, data in Figure 2 suggest that cells die in response to NMT inhibition through apoptosis.

A potentially important NMT substrate for the mode of action of cytotoxicity is the proto-oncogene c-Src, which is a validated target for cancer therapy.[30] Src family kinase inhibitors, such as dasatinib, can induce apoptosis and a G1 arrest as observed in the context of NMT inhibition, while high levels of c-Src tyrosine kinase activity have been associated with cancer progression, where they promote cell survival, proliferation, and metastasis.[31] *N*-myristoylation is required for the autophosphorylation of c-Src and, as a consequence, for its tyrosine kinase activity.[21] Upon NMT inhibition, we observed a decrease of phosphorylated c-Src after 1 day and 3 days, suggesting that c-Src had a reduced protein kinase activity, while levels of total c-Src remained constant (Supporting Information Figure S4). However, while c-Src is an interesting downstream target, we have previously shown that NMT has over 100 protein substrates in mammalian cells, and it is thus reasonable to suppose that additional proteins and pathways will be linked to the mode of action of NMT inhibition.

DOI: 10.1021/acschembio.6b00371
ACS Chem. Biol. 2016, 11, 2165−2176

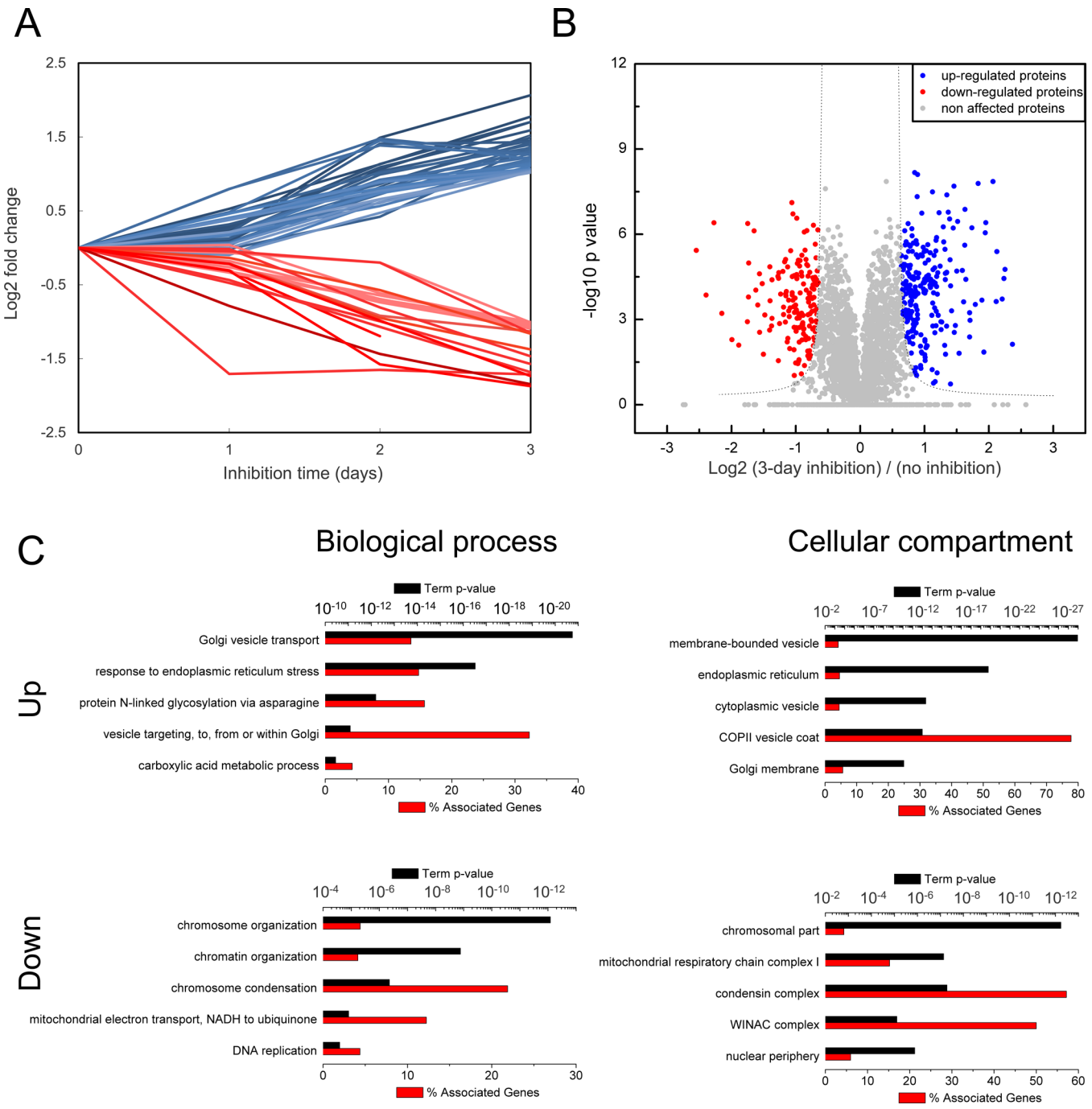

Figure 3. Quantitative proteomics and pathway analyses of NMT inhibited HeLa cells. (A) Dynamic profile of significantly altered protein levels. Cells were treated with DMSO control or inhibitor **1** (5 μM for 1, 2, or 3 days), and >1100 proteins were quantified across the four samples (n = 3 biological replicates).[3] Proteins for which abundance is significantly affected after 3 days of treatment and with a Log2 fold change >1 are shown (ANOVA, FDR < 0.05, s0 = 1). Red indicates significantly down-regulated proteins and blue significantly up-regulated proteins. (B) Volcano plot of log2 ratios representing log2 fold change of 3-day treatment to control, with lysate fractionation to increase proteome coverage (>3000 proteins quantified, n = 3 biological replicates). Dashed lines represent t test significance cutoff (Benjamini–Hochberg FDR 0.02, s0 of 1). A total of 398 proteins are differentially expressed at 3 days. Red indicates significantly down-regulated proteins. Blue shows significantly up-regulated proteins, and gray represents all other proteins. (C) GO annotations (biological process and cellular compartment) of proteins significantly up- and down-regulated after 3-day treatment, obtained from ClueGO and Cytoscape. The term p-value and the percentage of associated genes are indicated.

Global Analysis of Temporal Proteome Dynamics in Response to NMT Inhibition. We next sought to determine the progressive effects of NMT inhibition on key pathways in cells through whole proteome analysis. NMT inhibition induces negligible toxicity at 1 day, and we hypothesized that early mechanism-related changes in protein abundance might occur by 2 days, while after 3 days proteins affected by the inhibitor would reflect cell death pathways. We have previously shown that after 1-day treatment with inhibitor **1**,[3] the abundance of the large majority of proteins is not significantly affected. We thus performed a quantitative analysis of the proteome following treatment of HeLa cells with **1** (5 μM) for 0, 1, 2,

DOI: 10.1021/acschembio.6b00371
ACS Chem. Biol. 2016, 11, 2165–2176

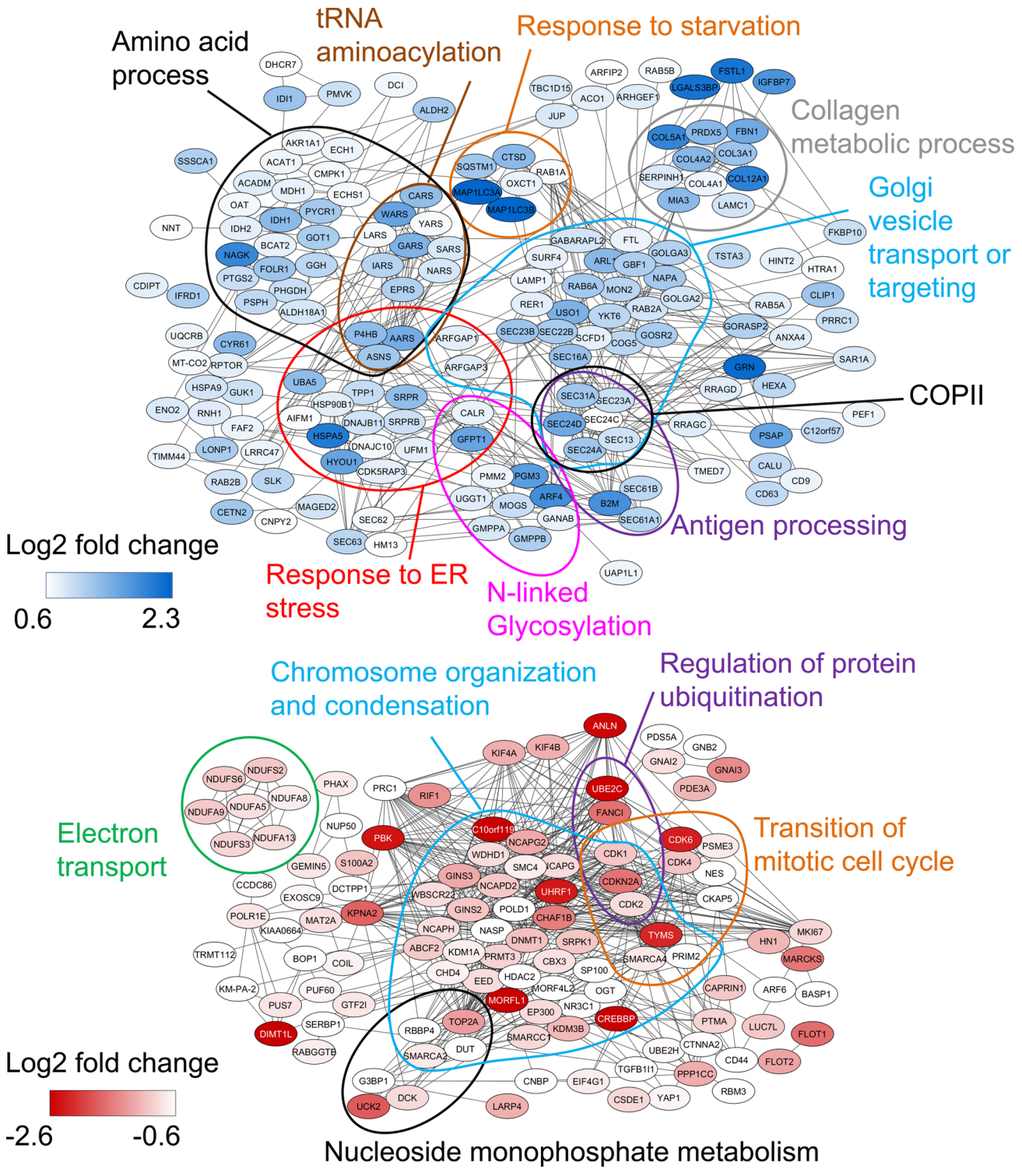

Figure 4. Proteome-wide expression changes upon NMT inhibition for 3 days in HeLa cells. Network analysis was performed with STRING and biological processes analyzed with ClueGo+. The interaction network was visualized with Cytoscape, and the most significantly enriched biological process clusters are indicated. (A) Network of up-regulated proteins. (B) Network of down-regulated proteins.

and 3 days using a Spike-in SILAC approach,[32] which allows quantitative comparison between multiple biological samples (n = 3 biological replicates) without restricting conditions for the experiment to media specific for isotopic labeling (Supporting Information Table 1). HeLa cells grown in standard DMEM media were treated with the inhibitor for 0−3 days and after lysis samples were spiked with lysate obtained from HeLa cells grown in media containing heavy Lys and Arg. Tryptic digestion of the samples using filter-assisted sample preparation (FASP)[33] enabled quantification of proteome-wide changes in protein abundance, determined in 3-fold replicate experiments at each of the four time points of inhibitor treatment on a high resolution nanoLC-MS/MS platform. A total of 1160 proteins were quantified in at least two replicates at each of the time

DOI: 10.1021/acschembio.6b00371
ACS Chem. Biol. 2016, 11, 2165−2176

points (Supporting Information Table 1 and Figure S5), with L/H ratios normalized to the median value in each sample. Proteins with a fold-change ratio of at least 2 (ANOVA-test, FDR < 0.05) after 3-day treatment compared to no treatment (0 day) are presented in Figure 3A. Twenty proteins were significantly down-regulated, while 37 proteins were up-regulated in response to NMT inhibition. Interestingly, the same groups of proteins were consistently and progressively down- or up-regulated over the course of the experiment, suggesting a consistent mechanism operating over time; these changes were strongest at 3 days, suggesting that the later time-point is most suitable to identify significantly affected proteins.

In order to obtain deeper protein quantification at 3 days, proteins were subjected to FASP and tryptic peptides fractionated by pipet-based strong anion exchange chromatography[34] prior to analysis by nanoLC-MS/MS. Three biological replicates were analyzed in 3 fractions for each time point (0 and 3 day treatment), leading to 18 data sets with excellent reproducibility between replicates (Pearson coefficient 0.816 to 0.921, Supporting Information Figure S6). More than 3500 proteins were identified, and 2749 proteins were accurately quantified in at least two replicates of both samples (Supporting Information Figure S6 and Table 2). The H/L ratio was normalized to the median over biological replicates, and the resultant quantitative distribution of relative protein abundance exhibited a broad spectrum of dynamics from −2.6 to +2.6 log2 fold change. In total, 398 differentially expressed proteins were identified with >1.5-fold change (*t* test significant, FDR = 0.02, s0 = 1) in the treated sample compared to control (Figure 3B), with 162 significantly down-regulated and 236 significantly up-regulated by NMT inhibition.

NMT Inhibition Induces ER-Stress in HeLa Cells. A combination of approaches was deployed to understand the biological functions most affected by NMT inhibition across the 398 differentially expressed proteins. The Cytoscape ClueGo plug-in (Figure 3C, Supporting Information Figure S7−S9 and Table 3) allowed functional grouping and visualization of nonredundant biological terms across the network, while analysis of the network using STRING enabled the main clusters of proteins to be obtained (Figure 4). NMT inhibition most significantly ($p < 10^{-4}$) down-regulated chromosome organization/condensation processes, consistent with cell cycle arrest, and mitochondrial electron transport (Figure 3C). The most significantly ($p < 10^{-10}$) up-regulated biological processes encompassed Golgi vesicle transport and the response to endoplasmic reticulum (ER) stress and carboxylic acid metabolism. In particular, proteins involved in activation of the unfolded protein response, protein *N*-glycosylation, and the ER-nucleus signaling pathway were strongly induced, including ER chaperone BiP,[35] which plays a central role in the folding and assembly of proteins, degradation of misfolded proteins, and preservation of ER homeostasis. A number of known BiP interacting proteins were also up-regulated, including other chaperones (GRP170/HYOU1) or cochaperones (DNAJC10), together with proteins involved in protein quality control (e.g., Calreticulin). Interestingly, the four other most significantly up-regulated biological processes are closely related to ER-stress. Notably, either activation of N-glycolysation by addition of N-glycan precursor N-acetylglucosamine or gain of function of GFAT/GFPT1 (which was overexpressed in the present study) were recently shown to activate the ER-associated degradation (ERAD) pathway and act as a protective mechanism by activating the clearance of misfolded proteins.[36]

NMT inhibition also resulted in significant up-regulation of proteins involved in incorporation of amino acids during protein translation, including aminoacyl-tRNA synthetases, amino acid transporters and proteins involved in the machinery of protein synthesis, such as tryptophan—tRNA ligase, cytoplasmic (WARS), serine—tRNA ligase, cytoplasmic (SARS), or bifunctional glutamate/proline-tRNA ligase (EPRS). This is consistent with induction of ER-stress, which has recently been shown to result in an increase in translation, and a potential mechanism for cell death.[37,38] Interestingly, we discovered significant up-regulation of five t-RNA ligase proteins, IARS, EPRS, GARS, AARS, and WARS, as well as seven proteins involved in the unfolded protein response, SEC31A, HSPA5, SRPR, AARS, GFPT1, HYOU1, and ASNS. To confirm induction of ER-stress following NMT inhibition, we analyzed cell lysates from HeLa cells treated with inhibitor **1** for 0, 1, 3, and 7 days by Western blot (Figure 5) and found

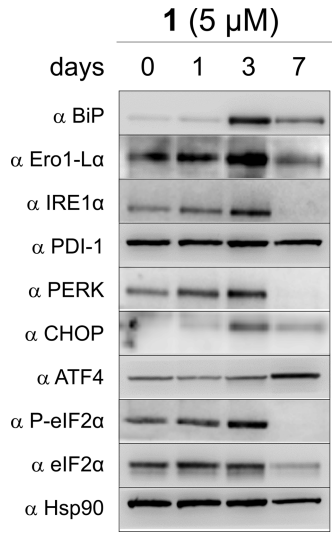

Figure 5. NMT inhibition induces ER stress in HeLa cells. Western blot analyses of markers of ER stress and unfolded protein response; HeLa were treated with inhibitor **1** (5 μM) for 0, 1, 3, or 7 days. Hsp90 was used as a loading control. Data are representative of at least three biological replicates.

that key markers of ER-stress, including BiP, Ero1-Lα, IRE1α, PDI-1, and PERK were relatively up-regulated in this cell line following NMT inhibition. Furthermore, CHOP, the pro-apoptotic transcription factor of the unfolded protein response (UPR), and proteins upstream of CHOP in the pro-apoptotic pathway of the UPR (PERK, eIF2α and ATF4) were also up-regulated (Figure 5), strongly suggesting that the UPR pathway contributes to activation of apoptosis.

NMT inhibition also appears to impact pathways relevant to ER to Golgi trafficking, a critical process involved in the sorting of properly folded, processed, and assembled proteins from unfolded or immature proteins, and from ER-resident proteins.[39] SEC23, SEC24, SEC13 and SEC31, SAR1a, and the components of COPII, which are associated with ER to the Golgi transport vesicles, are all up-regulated upon treatment with inhibitor **1**, as are COPII-associated proteins such as SLY1 (SCFD1) and melanoma inhibitory activity protein 3 (MIA3).[40,41]

DOI: 10.1021/acschembio.6b00371
ACS Chem. Biol. 2016, 11, 2165−2176

NMT Inhibition Induces a Related Phenotype in Other Cancer Cell Lines. As the proteome and myristoylated proteome of HeLa cells have been previously well-characterized, we initially employed this cell line to probe the mode of action of inhibitor **1**. In order to test the scope of this finding, MTS assays and cell cycle analyses were carried out for **1** in three additional cancer cell lines: MDA-MB-231 (breast cancer), HCT-116 (colon), and MCF-7 (breast; Supporting Information Figure 10A). The time-dependent response with residual metabolic activity characteristic of on-target NMT inhibition was found to be strongly conserved between these lines, suggesting a conserved mode of action through NMT inhibition. However, MDA-MB-231 and HCT-116 were not as sensitive to 3-day NMT inhibition, showing residual metabolic activities of 51% and 73%, respectively. MCF-7 also had a different pattern with a somewhat lower EC_{50} and a plateau of metabolic activity at 64%. Following prolonged NMT inhibition (7 days), treatment with 10 μM of inhibitor **1** resulted in cell death for all of these lines. In line with a conserved mode of action, all ER-stress markers previously probed in HeLa were also progressively up-regulated in all three cell lines, following NMT inhibition over 1, 3, and 7 days (Supporting Information Figure 10E).

Similarly to HeLa cells, MDA-MB-231, HCT-116, and MCF-7 underwent G1 accumulation after 1−2 days (Supporting Information Figure 10B−D). An increase in the number of subG0/G1 cells was also observed after 3 days for MCF-7 and MDA-MB-231 cells but not for HCT-116, suggesting that these cells might be less sensitive to NMT inhibition. NMT inhibition also induced apoptosis in MDA-MB-231, MCF-7, and HCT-116 cells; however, induction was slower in HCT-116, in agreement with the small sub G0/G1 population observed in cell cycle analysis (Supporting Information Figure 10C). These variations in sensitivity between lines may result from differential NMT substrate expression or NMT enzyme activity, the particular importance of specific NMT substrates in a given cell line, or differences in susceptibility to downstream cell death pathways (e.g., apoptosis).

DISCUSSION

In the present study, in-depth quantitative proteomics analysis was used to characterize the proteome-wide cellular response to NMT inhibition, identifying 398 significantly differentially expressed proteins. These changes were distributed across multiple important processes, with a substantial proportion converging on pathways related to cell cycle regulation and ER stress. The inhibitor used in the present study has been shown to be a selective pharmacological tool for inhibition of NMT activity in human cells.[3] Although we cannot categorically exclude a contribution from other targets, time-dependent cytotoxicity as well as a strong correlation between dose-dependent tagging of NMT substrate with YnMyr and dose-dependent cytotoxicity in HeLa are highly consistent with on-target and selective NMT inhibition in mammalian cells.[3]

ER-stress is a mechanism employed by cells to restore normal function of the ER following accumulation of misfolded proteins. Initially, proteins involved in protein folding or degradation (the unfolded protein response (UPR) pathway) are up-regulated, concurrent with an attenuation of translation of protein involved in the cell cycle and a G1 arrest,[42] in close agreement with observations made in the present study. During ER-stress, misfolded proteins are degraded in the ER associated degradation (ERAD) pathway by the proteasome, or alternatively by autophagy, which can act as a protective mechanism by helping cells to cope with ER-stress.[43] Several proteins involved in autophagy were up-regulated in the present study, including CTSD, GABARAPL2, LAMP1, MAP1LC3A, MAP1LC3B, MAP1LC3B2, RAB1A, and SQSTM1. If ER homeostasis is not restored, prolonged ER-stress will result in apoptosis and/or autophagy, and cell death,[44] and we observed that selective inhibition of NMT in HeLa cells resulted in progressive induction of ER stress and eventual cell death, at least in part through apoptosis. Interestingly, induction of ER-stress by tunicamycin, an N-glycosylation inhibitor widely employed to promote ER-stress, resulted in a comparable phenotype in neuroblastoma SH-SY5Y cells, with up-regulation of ER chaperones (BiP), aminoacyl-tRNA synthases, and proteins involved in protein transport, as well as induction of apoptosis.[45] NMT inhibition appeared to have a similar phenotype (G1 accumulation, increasing cell death over time, ER-stress) in a range of cancer cell lines, albeit with variations in sensitivity (Supporting Information Figure S10).

With more than 70 different proteins proven to be cotranslationally myristoylated by NMTs in HeLa cells, NMT inhibition is likely to affect multiple pathways, several of which could potentially trigger ER-stress. Notably, ADP-ribosylation factors (ARFs) are *N*-myristoylated small GTPases essential for COPI vesicle formation in retrograde protein transport from Golgi to ER.[46] *N*-myristoylation of ARF1 is required for binding to phospholipid membranes and activation by guanine nucleotide exchange factors (GEFs) that promote the exchange of GDP for GTP.[46,47] Inhibition of Golgi-specific Brefeldin A resistance factor 1 (GBF1), the ARF guanine nucleotide-exchange factor (GEF), by Brefeldin A prevents ARF activation and COPI recruitment to membranes, resulting in accumulation of proteins in the ER, ER-stress, and finally apoptosis.[46,48] Interestingly, GBF1 is also up-regulated in the present study, consistent with its recently reported role in responding to reduced ARF activity.[49] Taken together, these data suggest that ARFs merit future investigation as potentially important NMT substrates for the cytotoxic mode of action of NMT inhibitors. Arf1-targeted agents have recently been reported with potent *in vivo* anticancer activity,[50] and NMT inhibition is likely to result in a mechanistically distinct but functionally similar outcome by preventing Arf1 localization at the Golgi.

One of the 26S regulatory proteasome subunits (PSMC1) and four E3 ubiquitin ligases involved in the proteasome degradation pathway (MGRN1, RNF125, ZNRF1, and ZNRF2) are *N*-myristoylated, and ER-stress may also be enhanced following malfunction of the proteasome machinery. Indeed, Bortezomib A, a 26S proteasome inhibitor, is known to induce ER-stress by overloading the ERAD pathway with misfolded proteins.[43] During ER-stress, degradation of misfolded proteins by the proteasome (ERAD pathway) also allows recycling of essential amino acids in cells, and it was recently shown that proteasome inhibition can lead to cell death through the failure of amino acid homeostasis.[51] In this context, it is particularly interesting that starvation response processes were highly enriched ($p < 10^{-4}$) upon NMT inhibition.

It is also conceivable that NMT inhibition could result in accumulation of excess free myristic acid as a result of lowered flux through the *N*-myristoylation pathway. Although longer chain fatty acids have been observed to enhance ER-stress,[52] this mechanism seems unlikely to contribute to the mode of

DOI: 10.1021/acschembio.6b00371
ACS Chem. Biol. 2016, 11, 2165−2176

action in cells since introduction of excess myristic acid is minimally cytotoxic in comparison to longer chain fatty acids.[53]

CONCLUSION

The present study provides a resource to guide future targeting of specific diseases with NMT inhibitors and a preliminary study of the pathways affected by an NMT inhibitor as a single agent in cancer cells. While most of the pathways highlighted in our whole proteome analysis may be important for phenotypes other than cytotoxicity, we have shown that NMT inhibition kills HeLa cells at least in part through the ER stress and UPR pathways.

ER stress has been shown to be chronically activated in many tumors, where it allows tumor cells to proliferate and survive under extreme conditions such as hypoxia and protects them from chemotherapy.[54] Pharmacological ER stress can impose an additional burden on this pro-survival pathway, activating pro-apoptotic pathways and cell death. Several drugs promoting ER-stress have already entered the clinic, or are in clinical trials, such as Bortezomib A or Brefeldin A, discussed above.[55] However, these compounds can either increase sensitivity or resistance to anticancer therapies, depending on the inhibitor and the cancer cell line.[56] As both the proteasome and autophagy are important in the response to ER-stress to degrade unfolded proteins, it has been suggested that it might be beneficial to modulate these pathways simultaneously,[56] and NMT inhibitors offer a novel combination of ER-stress promoting mechanisms. In future studies it will be interesting to test the hypothesis that cell lines dependent on chronic ER-stress to survive will be particularly sensitive to NMT inhibition as a single agent, subject to cell-line-specific susceptibility to apoptosis. In contrast, normal and slowly proliferating cells that lack pre-existing ER stress could be less susceptible.

Taken together, the data presented here suggest that NMT inhibition progressively induces a unique and specific cell state through alteration of pathways connected to its 100+ substrate proteins. We have highlighted some of the most prominent pathways affected following extended inhibitor exposure, but it is also clear that the influence of NMT inhibition is remarkably subtle, with only 14% of the proteome significantly modulated after 3 days. We suggest that two complementary approaches could be used in the future to unlock the potential of NMT inhibitors for oncology indications: (1) wider screening of cancer cell line panels to uncover unanticipated sensitivities for specific cancer subtypes and (2) comparative proteomic analysis of NMT substrate profiles and proteome changes in contrasting or drug-resistant cell lines, to reveal sensitivity or resistance mechanisms. We anticipate that deeper system level analysis of these data sets will lead not only to novel indications for human NMT inhibitors as single agents but also to identification of drug synergies that exploit the altered signaling network induced by NMT inhibition to reverse resistance, improve efficacy, or extend the therapeutic index for agents already in the clinic.

METHODS

General. In-gel fluorescence was recorded using an ETTAN Dige Imager (GE Healthcare). Chemiluminescence was recorded using a LAS-3000 Imaging System (Fujifilm). Absorbance in 96-well plates was measured using a SpectraMax M2/M2e Microplate Reader from Molecular devices. Culture media and reagents were obtained from Sigma-Aldrich, Gibco (Life technologies) and A&E Scientific (PAA). For quantitative proteomics (SILAC), R10K8 and R0K0 DMEM media were purchased from Dundee cell products, and the cell dissociation buffer (enzyme free, PBS-based) was obtained from Gibco (Life Technologies). Dialyzed FBS was obtained from Sigma-Aldrich. All buffers were filtered using a 0.2 μM filter to prevent any contamination. MTS assay was performed as previously described.[3]

Cell Culture. HeLa, MDA-MB-231, and MCF-7 cells were grown in DMEM supplemented with 10% FBS and 1% penicillin/streptomycin. HCT 116 cells were grown in McCoy's 5a Medium Modified supplemented with 0.22 g/L glutamine, 10% FBS, and 1% penicillin/streptomycin. All cells were grown in a humidified 10% CO_2-containing atmosphere at 37 °C. Cells were plated 24 h before treatments. The number of cells plated for each cell line can be found in the Supporting Information.

Inhibitor 1 Treatment. Cells were incubated with inhibitor **1** (0, 1, or 5 μM) for 0−7 days before cell lysis (Western blot analysis), cell fixation (flow cytometry experiments), or treatment with MTS (cell cytotoxicity assay). The total amount of DMSO was normalized to the maximum amount of DMSO used.

Western Blot. After treatment with inhibitor **1**, cells were washed with PBS (3×) and lysed on ice (lysis buffer for apoptosis samples: PBS 1×, 0.1% SDS, 1% Triton X-100, 1 × EDTA-free complete protease inhibitor (Roche Diagnostics), and lysis buffer for ER stress/UPR samples: 100 mM tris at pH 7.4, 4% SDS, EDTA-free protease inhibitor). Lysates were kept on ice for 20 min and centrifuged at 17 000g for 20 min to remove insoluble material. Supernatants were collected and stored at −80 °C. Protein concentration was determined using the Bio-Rad DC Protein Assay. Proteins were separated on an SDS-PAGE gel and transferred to PVDF membranes (Millipore, Immobilon-PSQ membrane, pore size 0.2 μM) or nitrocellulose membranes (GE Healthcare, Hybond ECL, pore size 0.45 μM) using a wet transfer setup and a Tris-glycine transfer buffer supplemented with 0.1% SDS and 10% MeOH. Membranes were washed with TBS-T (1 × TBS, 0.1% Tween-20), blocked (5% dried skimmed milk in TBS-T), washed with TBS-T (3×), and then incubated with the appropriate primary antibody [BiP (Cell Signaling Technology, 9956S), Ero1-Lα (Cell Signaling Technology, 9956S), IRE1α (Cell Signaling Technology, 9956S), PDI (Cell Signaling Technology, 9956S), PERK (Cell Signaling Technology, 9956S), c-Src (Cell Signaling Technology, 2123), Tubulin (Santa Cruz, SC53646), pro-caspase 3 (Cell Signaling Technology SC13156), NMT1 (Atlas Antibodies, HPA022963), BID (Cell Signaling Technology 2002S), PARP (Santa Cruz, SC8007), CHOP (Cell Signaling Technology, 2895), Hsp90 (Santa Cruz, sc-69703), eIF2α (Cell Signaling Technology, 9722), phosphor-eIF2α (Cell Signaling Technology, 9721), or ATF4 (Proteintech, 10835-1-AP)] in blocking solution overnight, washed with TBS-T (4×, 10 min), incubated with the appropriate secondary antibodies in blocking solution for 1 h (mouse: HRP goat anti mouse, 1/20 000, BD Pharmingen, cat. no. 554002; rabbit: HRP goat anti rabbit, 1/5000, Invitrogen, cat. no. G-21234) washed with TBS-T (4×, 10 min) and developed with Luminata Crescendo Western HRP substrate (Millipore) according to the manufacturer's instructions and on a Fujifilm LAS 3000 imager.

Cell Cycle Analysis/PI Stain. After treatment with inhibitor **1** or DMSO, both adherent and floating cells were harvested and washed with PBS (2 × 1 mL). Cell pellets were resuspended in 70% EtOH and fixed overnight at 4 °C or for several days at −20 °C. Fixed cells were washed with PBS (2 × 1 mL). Cell pellets were resuspended in PI solution (200 μL, 50 μg/mL) and transferred to a 5 mL tube for flow cytometry analysis. A total of 10 μL of RNase was added to each tube. Samples were quickly vortexed and incubated at RT in the dark prior to analysis. Samples were processed using a BD LSRFortessa cell analyzer (BD Biosciences, UK). The distribution of cells in each phase of the cell cycle was calculated using FlowJo 7.6.5 software.

Annexin V/PI Analysis. Dead and apoptotic cells were detected using an FITC Annexin V Apoptosis Detection Kit I (BD Pharmingen) and the protocol described by the supplier with some modifications.

After treatment with the inhibitor or DMSO, both adherent and floating cells were harvested and washed with PBS (2 × 1 mL). Cell pellets were resuspended in 200 μL of 1× binding buffer (1 × 10^6

DOI: 10.1021/acschembio.6b00371
ACS Chem. Biol. 2016, 11, 2165−2176

cells/mL). A total of 100 μL of the solution were transferred to a 5 mL tube. A total of 5 μL of FITC Annexin V and 5 μL PI were added. The samples were vortexed and incubated for 15 min at RT in the dark. A total of 400 μL of 1× binding buffer was added to each tube prior to analysis by flow cytometry. Samples were analyzed within 1 h following PI and Annexin V addition. Samples were processed using a BD LSRFortessa cell analyzer (BD Biosciences, UK). Samples were compensated automatically using untreated cells and unstained, apoptotic cells (1 μM STS treatment for 6 h) stained with Annexin V and dead cells (10 μM treated cells for 7 days) stained with PI.

The distribution of apoptotic, dead, and alive cells was calculated using FlowJo 7.6.5 software.

BrdU/PI Stain. Cells were treated with BrdU (10 mM, GE Healthcare) for 30 min before the end of the experiment. Both adherent and floating cells were harvested and washed with PBS (1 × 1 mL). Cell pellets were resuspended in 70% EtOH and fixed overnight at 4 °C or for several days at −20 °C. Fixed cells were washed with PBS (1 × 1 mL) and collected by centrifugation. Cells were resuspended in 2 M HCl/0.5% (v/v) Triton X-100 and incubated at RT for 30 min.

Cells were collected by centrifugation, washed in 1 mL of neutralizing solution (0.1 M Tris at pH 8.5), and collected once more before addition of 1 mL of blocking solution (1% (w/v) BSA/0.5% (v/v) Tween 20 in PBS). A total of 10^6 cells were transferred to a Falcon tube and collected by centrifugation. Cells were resuspended directly in a solution of the FITC-conjugated anti-BrdU antibody (347583, BD Biosciences, 1 μL) in blocking solution (1% (w/v) BSA/0.5% (v/v) Tween 20 in PBS, 19 μL) and incubated at RT in the dark for 30 min. Cells were then washed with blocking solution and collected by centrifugation. Cell pellets were resuspended in PI solution (200 μL, 50 μg/mL) and transferred to a 5 mL tube for flow cytometry analysis. A total of 10 μL of RNase was added to each tube. Samples were incubated at RT in the dark prior to analysis. FITC-fluorescence against PI fluorescence using the FlowJo 7.6.5 software. BrdU positive cells were scored as the population of cells with FITC-fluorescence higher than that of the G1 or G2/M population

Proteomics: Cells ± Inhibitor. Following treatment with inhibitor **1** for 0, 1, 2, or 3 days (5 μM), adherent and floating cells were lysed in 100 mM Tris at pH 7.4, 4% SDS, 0.1 M DTT EDTA-free protease inhibitor. Protein concentration was determined, and the samples were spiked-in with a heavy spike-in standard prepared by lysing heavy HeLa cells in the same lysis buffer. The samples and spike-in standard were mixed in a 1:1 ratio. Samples were digested according to a Filter-Aided Sample Preparation (FASP) protocol, which was performed using a 5 kDa molecular weight cutoff filter (EMD Millipore), according to Sharma *et al.*[26] with modifications. Briefly, 30 μL of each sample (60 μg of lysate) was mixed with 200 μL of 8 M urea in 100 mM Tris-HCl (pH 8.5; urea buffer) in the spin filter and centrifuged at 14 000*g* for 15 min at 20 °C to remove SDS. The centrifugation steps were repeated if the volume left in the filter exceeded 50 μL. The proteins were washed with 200 μL of urea buffer to exchange any remaining SDS by urea. The proteins were alkylated with 100 μL of 50 mM iodoacetamide for 20 min at RT in the dark. The proteins were washed with urea buffer (2 × 100 μL) and with 50 mM ammonium bicarbonate (pH 8.0; 5 × 200 μL). A total of 1 μg of trypsin in 100 μL of 50 mM ammonium bicarbonate (pH 8.0) was added to the proteins in the spin filter, and proteins were digested with trypsin overnight at 37 °C. Peptides were eluted by centrifugation by the addition of 40 μL of 50 mM ammonium bicarbonate (pH 8.0) and of 50 μL of 0.5 M NaCl. Where indicated, samples were fractionated to increase the number of identified proteins according to a published protocol.[34] Samples were acidified with TFA (1% (v/v) TFA) and loaded on the sorbent and washed with 0.2% (v/v) TFA in Milli-Q water (2 × 60 μL) to desalt the sample. Elution occurred from the sorbent (SDB-RPS from 3M) with 60 μL of 100 mM ammonium formate, 40% (v/v) ACN, and 0.5% (v/v) formic acid to give "fraction 1," with 60 μL of 5% (v/v) ammonium hydroxide and 80% (v/v) ACN to yield "fraction 2," followed by elution with 60 μL 5% (v/v) ammonium hydroxide and 80% (v/v) ACN to give "fraction 3." Fractions were concentrated and peptides dissolved in 0.5% TFA and 2% acetonitrile in water before being transferred into LC-MS sample vials. Nonfractionated samples were desalted prior to LC-MS/MS analysis according to a published protocol.[57] Elution from the sorbent (SDC-XC from 3M) with 70% acetonitrile in water was followed by speed-vac-assisted solvent removal, reconstitution of peptides in 0.5% TFA, and 2% acetonitrile in water and transferred into LC-MS sample vials.

LC-MS/MS Analysis. The analysis was performed as previously described[3] using an Acclaim PepMap RSLC column (50 cm × 75 μm inner-diameter; Thermo Fisher Scientific) using a 2 h acetonitrile gradient in 0.1% aqueous formic acid at a flow rate of 250 nL min^{-1}. Easy nLC-1000 was coupled to a Q Exactive mass spectrometer *via* an easy-spray source (all Thermo Fisher Scientific). The Q Exactive was operated in data-dependent mode with survey scans acquired at a resolution of 75 000 at m/z 200 (transient time 256 ms). Up to 10 of the most abundant isotope patterns with a charge of +2 or higher from the survey scan were selected with an isolation window of 3.0 m/z and fragmented by higher-energy collision dissociation (HCD) with normalized collision energies of 25. The maximum ion injection times for the survey scan and the MS/MS scans (acquired with a resolution of 17 500 at m/z 200) were 20 and 120 ms, respectively. The ion target value for MS was set to 106 and for MS/MS to 105, and the intensity threshold was set to 8.3 × 102.

Proteomics Data Analysis. The data were processed with MaxQuant version 1.3.0.5,[58] and the peptides were identified from the MS/MS spectra searched against the human Swissprot+Isoforms database (July 2013) using the Andromeda search engine. Cysteine carbamidomethylation was used as a fixed modification and methionine oxidation as a variable modification. Up to two missed cleavages were allowed. "Unique and razor peptides" mode was selected. The FDR was set to 0.01 for peptides, proteins, and sites. Other parameters were used as preset in the software. Data were analyzed using Microsoft Office Excel 2007 and Perseus version 1.3.0.4.

Analysis of the Nonfractionated Samples. The experiment comprised three biological replicates for each sample (0 day treatment, 1 day treatment, 2 day treatment, 3 day treatment). The replicates were grouped together. Ratios of light/heavy (L/H, corresponding to the amount of protein in the lysate treated with the inhibitor for 0−3 days/amount of protein in the spike-in standard) found for each protein, each condition, and each replicate (three biological replicates) were determined by MaxQuant as explained above. The data were filtered to require at least two valid values in the "0 day treatment" protein group. Ratios were logarithmized (base 2). L/H ratios were normalized to the median value in each replicate. An ANOVA test was performed to detect significant changes between the four time points (permutation based FDR statistics were applied (250 permutation, FDR < 0.05, 2 tailed, s0 = 1). The data were filtered to keep only proteins which were significantly up/down regulated based on the ANOVA test. The data were further filtered by keeping only the proteins with a Log2 fold change higher than 1 ("up-regulated" proteins) or lower than −1 ("down-regulated" proteins) after 3 days (for protein with no valid value in the 3 day samples, the data were manually inspected, and protein with a Log2 fold change higher than 1 (or lower than −1) after 2 days was added to the list of significant proteins). To get the Log2 fold change after 1 day treatment, 2 day treatment, and 3 day treatment, the Log2 mean of L/H ratios for "0 day treatment" was subtracted from the mean of L/H ratios of the 1 day treatment, 2 day treatment, and 3 day treatment, respectively.

Analysis of the Fractionated Samples. For the fractionated samples (three fractions/replicate, three biological replicate for each sample (0 day treatment and 3 day treatment), 18 LC-MS runs in total), fractions of a same biological replicate were combined using the "set fractions" function in MaxQuant. The data were filtered to require at least one valid value. The replicates were grouped together. Ratios of light/heavy (L/H, corresponding to amount of protein in the lysate treated with the inhibitor for 0−3 days/amount of protein in the spike-in standard) found for each protein, each condition, and each replicate (three biological replicates) were determined by MaxQuant as explained above. L/H ratios were normalized to the median value in

DOI: 10.1021/acschembio.6b00371
ACS Chem. Biol. 2016, 11, 2165−2176

each sample. A modified *t* test with permutation based FDR statistics was applied ("two-sample test," FDR of 0.02, s0 = 1) between the two groups. Protein interaction networks were generated with STRING 9.1[59] and visualized with Cytoscape 3.2.0.[60] Biological processes were analyzed with ClueGo 2.1.5.[61]

■ ASSOCIATED CONTENT

Supporting Information

The Supporting Information is available free of charge on the ACS Publications website at DOI: 10.1021/acschembio.6b00371.

Additional methods, supplementary figures and complete data table of proteomics experiments (PDF)
Table 1 (XLSX)
Table 2 (XLSX)
Table 3 (XLSX)

■ AUTHOR INFORMATION

Corresponding Author

*Phone: +44 (0) 2075943752. E-mail: e.tate@imperial.ac.uk.

Present Address

[‖]The Rockefeller University, 1230 York Avenue, New York, USA

Notes

The authors declare no competing financial interest.

Proteomics mass spectrometry data sets have been deposited with the ProteomeXchange Consortium[62] *via* the PRIDE partner repository, with the data set identifier PXD003186.

■ ACKNOWLEDGMENTS

The authors thank Ute Brassat, Goska Broncel, and Remigiusz Serwa for helpful discussion. This work was supported by Cancer Research UK (grants C29637/A10711, C29637/A9913, and C29637/A20183), and the Biotechnology and Biological Sciences Research Council (BB/D02014X/1).

■ REFERENCES

(1) Boutin, J. A. (1997) Myristoylation. *Cell. Signalling 9*, 15−35.

(2) Wright, M. H., Heal, W. P., Mann, D. J., and Tate, E. W. (2010) Protein myristoylation in health and disease. *J. Chem. Biol. 3*, 19−35.

(3) Thinon, E., Serwa, R. A., Broncel, M., Brannigan, J. A., Brassat, U., Wright, M. H., Heal, W. P., Wilkinson, A. J., Mann, D. J., and Tate, E. W. (2014) Global profiling of co- and post-translationally N-myristoylated proteomes in human cells. *Nat. Commun. 5*, 4919.

(4) Frearson, J. A., Brand, S., McElroy, S. P., Cleghorn, L. A. T., Smid, O., Stojanovski, L., Price, H. P., Guther, M. L. S., Torrie, L. S., Robinson, D. A., Hallyburton, I., Mpamhanga, C. P., Brannigan, J. A., Wilkinson, A. J., Hodgkinson, M., Hui, R., Qiu, W., Raimi, O. G., van Aalten, D. M. F., Brenk, R., Gilbert, I. H., Read, K. D., Fairlamb, A. H., Ferguson, M. A. J., Smith, D. F., and Wyatt, P. G. (2010) N-myristoyltransferase inhibitors as new leads to treat sleeping sickness. *Nature 464*, 728−732.

(5) Wright, M. H., Paape, D., Storck, E. M., Serwa, R. A., Smith, D. F., and Tate, E. W. (2015) Global analysis of protein N-myristoylation and exploration of N-myristoyltransferase as a drug target in the neglected human pathogen Leishmania donovani. *Chem. Biol. 22*, 342−54.

(6) Hutton, J. A., Goncalves, V., Brannigan, J. A., Paape, D., Wright, M. H., Waugh, T. M., Roberts, S. M., Bell, A. S., Wilkinson, A. J., Smith, D. F., Leatherbarrow, R. J., and Tate, E. W. (2014) Structure-based design of potent and selective Leishmania N-myristoyltransferase inhibitors. *J. Med. Chem. 57*, 8664−70.

(7) Wright, M. H., Clough, B., Rackham, M. D., Rangachari, K., Brannigan, J. A., Grainger, M., Moss, D. K., Bottrill, A. R., Heal, W. P., Broncel, M., Serwa, R. A., Brady, D., Mann, D. J., Leatherbarrow, R. J., Tewari, R., Wilkinson, A. J., Holder, A. A., and Tate, E. W. (2014) Validation of N-myristoyltransferase as an antimalarial drug target using an integrated chemical biology approach. *Nat. Chem. 6*, 112−121.

(8) Rackham, M. D., Brannigan, J. A., Rangachari, K., Meister, S., Wilkinson, A. J., Holder, A. A., Leatherbarrow, R. J., and Tate, E. W. (2014) Design and synthesis of high affinity inhibitors of Plasmodium falciparum and Plasmodium vivax N-myristoyltransferases directed by ligand efficiency dependent lipophilicity (LELP). *J. Med. Chem. 57*, 2773−88.

(9) Yu, Z., Brannigan, J. A., Moss, D. K., Brzozowski, A. M., Wilkinson, A. J., Holder, A. A., Tate, E. W., and Leatherbarrow, R. J. (2012) Design and synthesis of inhibitors of Plasmodium falciparum N-myristoyltransferase, a promising target for antimalarial drug discovery. *J. Med. Chem. 55*, 8879−90.

(10) Goncalves, V., Brannigan, J. A., Whalley, D., Ansell, K. H., Saxty, B., Holder, A. A., Wilkinson, A. J., Tate, E. W., and Leatherbarrow, R. J. (2012) Discovery of Plasmodium vivax N-myristoyltransferase inhibitors: screening, synthesis, and structural characterization of their binding mode. *J. Med. Chem. 55*, 3578−82.

(11) Fang, W., Robinson, D. A., Raimi, O. G., Blair, D. E., Harrison, J. R., Lockhart, D. E. A., Torrie, L. S., Ruda, G. F., Wyatt, P. G., Gilbert, I. H., and van Aalten, D. M. F. (2015) N-Myristoyltransferase Is a Cell Wall Target in Aspergillus fumigatus. *ACS Chem. Biol. 10*, 1425−1434.

(12) Bell, A. S., Mills, J. E., Williams, G. P., Brannigan, J. A., Wilkinson, A. J., Parkinson, T., Leatherbarrow, R. J., Tate, E. W., Holder, A. A., and Smith, D. F. (2012) Selective Inhibitors of Protozoan Protein N-myristoyltransferases as Starting Points for Tropical Disease Medicinal Chemistry Programs. *PLoS Neglected Trop. Dis. 6*, e1625.

(13) Tate, E. W., Bell, A. S., Rackham, M. D., and Wright, M. H. (2014) N-Myristoyltransferase as a potential drug target in malaria and leishmaniasis. *Parasitology 141*, 37−49.

(14) Wright, M. H., Paape, D., Price, H. P., Smith, D. F., and Tate, E. W. (2016) Global profiling and inhibition of protein lipidation in vector and host stages of the sleeping sickness parasite Trypanosoma brucei. *ACS Infect. Dis.*, DOI: 10.1021/acsinfecdis.6b00034.

(15) Giang, D. K., and Cravatt, B. F. (1998) A second mammalian N-myristoyltransferase. *J. Biol. Chem. 273*, 6595−6598.

(16) Rampoldi, F., Bonrouhi, M., Boehm, M. E., Lehmann, W. D., Popovic, Z. V., Kaden, S., Federico, G., Brunk, F., Gröne, H.-J., and Porubsky, S. (2015) Immunosuppression and Aberrant T Cell Development in the Absence of N-Myristoylation. *J. Immunol. 195*, 4228−43.

(17) Felsted, R. L., Glover, C. J., and Hartman, K. (1995) Protein N-myristoylation as a chemotherapeutic target for cancer. *J. Natl. Cancer Inst. 87*, 1571−1573.

(18) Selvakumar, P., Lakshmikuttyamma, A., Shrivastav, A., Das, S. B., Dimmock, J. R., and Sharma, R. K. (2007) Potential role of N-myristoyltransferase in cancer. *Prog. Lipid Res. 46*, 1−36.

(19) Tate, E. W., Kalesh, K. A., Lanyon-Hogg, T., Storck, E. M., and Thinon, E. (2015) Global profiling of protein lipidation using chemical proteomic technologies. *Curr. Opin. Chem. Biol. 24*, 48−57.

(20) Broncel, M., Serwa, R. A., Ciepla, P., Krause, E., Dallman, M. J., Magee, A. I., and Tate, E. W. (2015) Multifunctional Reagents for Quantitative Proteome-Wide Analysis of Protein Modification in Human Cells and Dynamic Profiling of Protein Lipidation During Vertebrate Development. *Angew. Chem., Int. Ed. 54*, 5948−51.

(21) Patwardhan, P., and Resh, M. D. (2010) Myristoylation and membrane binding regulate c-Src stability and kinase activity. *Mol. Cell. Biol. 30*, 4094−4107.

(22) Liang, J., Xu, Z.-X., Ding, Z., Lu, Y., Yu, Q., Werle, K. D., Zhou, G., Park, Y.-Y., Peng, G., Gambello, M. J., and Mills, G. B. (2015) Myristoylation confers noncanonical AMPK functions in autophagy selectivity and mitochondrial surveillance. *Nat. Commun. 6*, 7926.

(23) Kimura, A., Kato, Y., and Hirano, H. (2012) N-myristoylation of the Rpt2 subunit regulates intracellular localization of the yeast 26S proteasome. *Biochemistry 51*, 8856−8866.

DOI: 10.1021/acschembio.6b00371
ACS Chem. Biol. 2016, 11, 2165−2176

(24) Kimura, A., Kurata, Y., Nakabayashi, J., Kagawa, H., and Hirano, H. (2016) N-Myristoylation of the Rpt2 subunit of the yeast 26S proteasome is implicated in the subcellular compartment-specific protein quality control system. *J. Proteomics 130*, 33−41.
(25) Medina-Ramirez, C. M., Goswami, S., Smirnova, T., Bamira, D., Benson, B., Ferrick, N., Segall, J., Pollard, J. W., and Kitsis, R. N. (2011) Apoptosis inhibitor ARC promotes breast tumorigenesis, metastasis, and chemoresistance. *Cancer Res. 71*, 7705−7715.
(26) Sharma, K., Vabulas, R. M., Macek, B., Pinkert, S., Cox, J., Mann, M., and Hartl, F. U. (2012) Quantitative proteomics reveals that Hsp90 inhibition preferentially targets kinases and the DNA damage response. *Mol. Cell. Proteomics 11*, M111 014654.
(27) Krönke, J., Udeshi, N. D., Narla, A., Grauman, P., Hurst, S. N., McConkey, M., Svinkina, T., Heckl, D., Comer, E., Li, X., Ciarlo, C., Hartman, E., Munshi, N., Schenone, M., Schreiber, S. L., Carr, S. A., and Ebert, B. L. (2014) Lenalidomide causes selective degradation of IKZF1 and IKZF3 in multiple myeloma cells. *Science 343*, 301−5.
(28) Chae, H.-J., Kang, J.-S., Byun, J.-O., Han, K.-S., Kim, D.-U., Oh, S.-M., Kim, H.-M., Chae, S.-W., and Kim, H.-R. (2000) Molecular mechanism of staurosporine-induced apoptosis in osteoblasts. *Pharmacol. Res. 42*, 373−381.
(29) Perinpanayagam, M. A., Beauchamp, E., Martin, D. D., Sim, J. Y., Yap, M. C., and Berthiaume, L. G. (2013) Regulation of co- and post-translational myristoylation of proteins during apoptosis: interplay of N-myristoyltransferases and caspases. *FASEB J. 27*, 811−821.
(30) Aleshin, A., and Finn, R. S. (2010) SRC: a century of science brought to the clinic. *Neoplasia 12*, 599−607.
(31) Wheeler, D. L., Iida, M., and Dunn, E. F. (2009) The role of Src in solid tumors. *Oncologist 14*, 667−678.
(32) Geiger, T., Wisniewski, J. R., Cox, J., Zanivan, S., Kruger, M., Ishihama, Y., and Mann, M. (2011) Use of stable isotope labeling by amino acids in cell culture as a spike-in standard in quantitative proteomics. *Nat. Protoc. 6*, 147−157.
(33) Wisniewski, J. R., Zougman, A., Nagaraj, N., and Mann, M. (2009) Universal sample preparation method for proteome analysis. *Nat. Methods 6*, 359−362.
(34) Kulak, N. A., Pichler, G., Paron, I., Nagaraj, N., and Mann, M. (2014) Minimal, encapsulated proteomic-sample processing applied to copy-number estimation in eukaryotic cells. *Nat. Methods 11*, 319−24.
(35) Dudek, J., Benedix, J., Cappel, S., Greiner, M., Jalal, C., Müller, L., and Zimmermann, R. (2009) Functions and pathologies of BiP and its interaction partners. *Cell. Mol. Life Sci. 66*, 1556−69.
(36) Denzel, M. S., Storm, N. J., Gutschmidt, A., Baddi, R., Hinze, Y., Jarosch, E., Sommer, T., Hoppe, T., and Antebi, A. (2014) Hexosamine pathway metabolites enhance protein quality control and prolong life. *Cell 156*, 1167−78.
(37) Krokowski, D., Han, J., Saikia, M., Majumder, M., Yuan, C. L., Guan, B.-J., Bevilacqua, E., Bussolati, O., Bröer, S., Arvan, P., Tchórzewski, M., Snider, M. D., Puchowicz, M., Croniger, C. M., Kimball, S. R., Pan, T., Koromilas, A. E., Kaufman, R. J., and Hatzoglou, M. (2013) A self-defeating anabolic program leads to β-cell apoptosis in endoplasmic reticulum stress-induced diabetes via regulation of amino acid flux. *J. Biol. Chem. 288*, 17202−13.
(38) Han, J., Back, S. H., Hur, J., Lin, Y.-H., Gildersleeve, R., Shan, J., Yuan, C. L., Krokowski, D., Wang, S., Hatzoglou, M., Kilberg, M. S., Sartor, M. A., and Kaufman, R. J. (2013) ER-stress-induced transcriptional regulation increases protein synthesis leading to cell death. *Nat. Cell Biol. 15*, 481−90.
(39) Geva, Y., and Schuldiner, M. (2014) The back and forth of cargo exit from the endoplasmic reticulum. *Curr. Biol. 24*, R130−6.
(40) Jensen, D., and Schekman, R. (2011) COPII-mediated vesicle formation at a glance. *J. Cell Sci. 124*, 1−4.
(41) Malhotra, V., Erlmann, P., and Nogueira, C. (2015) Procollagen export from the endoplasmic reticulum. *Biochem. Soc. Trans. 43*, 104−7.
(42) Brewer, J. W., Hendershot, L. M., Sherr, C. J., and Diehl, J. A. (1999) Mammalian unfolded protein response inhibits cyclin D1 translation and cell-cycle progression. *Proc. Natl. Acad. Sci. U. S. A. 96*, 8505−8510.
(43) Verfaillie, T., Salazar, M., Velasco, G., and Agostinis, P. (2010) Linking ER Stress to Autophagy: Potential Implications for Cancer Therapy. *Int. J. Cell Biol. 2010*, 930509.
(44) Hetz, C. (2012) The unfolded protein response: controlling cell fate decisions under ER stress and beyond. *Nat. Rev. Mol. Cell Biol. 13*, 89−102.
(45) Bull, V. H., and Thiede, B. (2012) Proteome analysis of tunicamycin-induced ER stress. *Electrophoresis 33*, 1814−23.
(46) Beck, R., Rawet, M., Ravet, M., Wieland, F. T., and Cassel, D. (2009) The COPI system: molecular mechanisms and function. *FEBS Lett. 583*, 2701−9.
(47) Goldberg, J. (1998) Structural basis for activation of ARF GTPase: mechanisms of guanine nucleotide exchange and GTP-myristoyl switching. *Cell 95*, 237−48.
(48) Citterio, C., Vichi, A., Pacheco-Rodriguez, G., Aponte, A. M., Moss, J., and Vaughan, M. (2008) Unfolded protein response and cell death after depletion of brefeldin A-inhibited guanine nucleotide-exchange protein GBF1. *Proc. Natl. Acad. Sci. U. S. A. 105*, 2877−82.
(49) Quilty, D., Gray, F., Summerfeldt, N., Cassel, D., and Melançon, P. (2014) Arf activation at the Golgi is modulated by feed-forward stimulation of the exchange factor GBF1. *J. Cell Sci. 127*, 354−64.
(50) Ohashi, Y., Iijima, H., Yamaotsu, N., Yamazaki, K., Sato, S., Okamura, M., Sugimoto, K., Dan, S., Hirono, S., and Yamori, T. (2012) AMF-26, a novel inhibitor of the Golgi system, targeting ADP-ribosylation factor 1 (Arf1) with potential for cancer therapy. *J. Biol. Chem. 287*, 3885−97.
(51) Suraweera, A., Munch, C., Hanssum, A., Bertolotti, A., Münch, C., Hanssum, A., and Bertolotti, A. (2012) Failure of amino acid homeostasis causes cell death following proteasome inhibition. *Mol. Cell 48*, 242−253.
(52) Cao, J., Dai, D.-L., Yao, L., Yu, H.-H., Ning, B., Zhang, Q., Chen, J., Cheng, W.-H., Shen, W., and Yang, Z.-X. (2012) Saturated fatty acid induction of endoplasmic reticulum stress and apoptosis in human liver cells via the PERK/ATF4/CHOP signaling pathway. *Mol. Cell. Biochem. 364*, 115−29.
(53) Niso-Santano, M., Malik, S. A., Pietrocola, F., Bravo-San Pedro, J. M., Mariño, G., Cianfanelli, V., Ben-Younès, A., Troncoso, R., Markaki, M., Sica, V., Izzo, V., Chaba, K., Bauvy, C., Dupont, N., Kepp, O., Rockenfeller, P., Wolinski, H., Madeo, F., Lavandero, S., Codogno, P., Harper, F., Pierron, G., Tavernarakis, N., Cecconi, F., Maiuri, M. C., Galluzzi, L., and Kroemer, G. (2015) Unsaturated fatty acids induce non-canonical autophagy. *EMBO J. 34*, 1025−41.
(54) Schonthal, A. H. (2012) Targeting endoplasmic reticulum stress for cancer therapy. *Front. Biosci., Scholar Ed. 4*, 412−31.
(55) Yadav, R. K., Chae, S.-W., Kim, H.-R., and Chae, H. J. (2014) Endoplasmic reticulum stress and cancer. *J. cancer Prev. 19*, 75−88.
(56) Nagelkerke, A., Bussink, J., Sweep, F. C. G. J., and Span, P. N. (2014) The unfolded protein response as a target for cancer therapy. *Biochim. Biophys. Acta, Rev. Cancer 1846*, 277−84.
(57) Rappsilber, J., Ishihama, Y., and Mann, M. (2003) Stop and Go Extraction Tips for Matrix-Assisted Laser Desorption/Ionization, Nanoelectrospray, and LC/MS Sample Pretreatment in Proteomics. *Anal. Chem. 75*, 663−670.
(58) Cox, J., and Mann, M. (2008) MaxQuant enables high peptide identification rates, individualized p.p.b.-range mass accuracies and proteome-wide protein quantification. *Nat. Biotechnol. 26*, 1367−1372.
(59) Franceschini, A., Szklarczyk, D., Frankild, S., Kuhn, M., Simonovic, M., Roth, A., Lin, J., Minguez, P., Bork, P., von Mering, C., and Jensen, L. J. (2013) STRING v9.1: protein-protein interaction networks, with increased coverage and integration. *Nucleic Acids Res. 41*, D808−15.
(60) Shannon, P., Markiel, A., Ozier, O., Baliga, N. S., Wang, J. T., Ramage, D., Amin, N., Schwikowski, B., and Ideker, T. (2003) Cytoscape: a software environment for integrated models of biomolecular interaction networks. *Genome Res. 13*, 2498−2504.
(61) Bindea, G., Mlecnik, B., Hackl, H., Charoentong, P., Tosolini, M., Kirilovsky, A., Fridman, W.-H., Pagès, F., Trajanoski, Z., and Galon, J. (2009) ClueGO: a Cytoscape plug-in to decipher

DOI: 10.1021/acschembio.6b00371
ACS Chem. Biol. 2016, 11, 2165−2176

functionally grouped gene ontology and pathway annotation networks. *Bioinformatics 25*, 1091−3.
(62) Vizcaíno, J. A., Deutsch, E. W., Wang, R., Csordas, A., Reisinger, F., Ríos, D., Dianes, J. A., Sun, Z., Farrah, T., Bandeira, N., Binz, P.-A., Xenarios, I., Eisenacher, M., Mayer, G., Gatto, L., Campos, A., Chalkley, R. J., Kraus, H.-J., Albar, J. P., Martinez-Bartolomé, S., Apweiler, R., Omenn, G. S., Martens, L., Jones, A. R., and Hermjakob, H. (2014) ProteomeXchange provides globally coordinated proteomics data submission and dissemination. *Nat. Biotechnol. 32*, 223−6.

DOI: 10.1021/acschembio.6b00371
ACS Chem. Biol. 2016, 11, 2165−2176